SI Appendix

Molecular mechanism for the recognition of sequence-divergent CIF peptides by the plant receptor kinases GSO1/SGN3 and GSO2.

Satohiro Okuda[1,*], Satoshi Fujita[2,*,#], Andrea Moretti[1], Ulrich Hohmann[1,+], Verónica G. Doblas[2,$], Yan Ma[2], Alexandre Pfister[2], Benjamin Brandt[1,&], Niko Geldner[2], Michael Hothorn[1]

Author affiliations

[1]Structural Plant Biology Laboratory, Department of Botany and Plant Biology, University of Geneva, 1211 Geneva, Switzerland.

[2]Department of Plant Molecular Biology, University of Lausanne, 1015 Lausanne, Switzerland.

[$]Present address: Institut Jean-Pierre Bourgin, INRA, AgroParisTech, CNRS, Université Paris-Saclay, 78000 Versailles, France.

[#]Present address: National Institute of Genetics, Mishima, Shizuoka 411-8540, Japan.

[+]Present address: Institute of Molecular Biotechnology of the Austrian Academy of Sciences (IMBA) & Research Institute of Molecular Pathology (IMP), Vienna Biocenter (VBC), 1030 Vienna, Austria.

[&]Present address: Department of Plant and Microbial Biology, University of Zurich, 8008 Zurich, Switzerland.

[*]these authors contributed equally to this work.

Corresponding Authors

To whom correspondence should be addressed: niko.geldner@unil.ch, michael.hothorn@unige.ch

Supplementary Materials and Methods

Protein expression and purification

The GSO1/SGN3 (residues 19 - 870) coding sequence was amplified from the AP018 plasmid containing SGN3 cDNA (1). GSO2 (residues 23 - 861), TPST (residues 25 - 441), SERK1 (residues 24 – 213), SERK3 (residues 1 – 220), NIK3 (residues 26 – 238), NIK4 (residues 31 – 238), SRF3 (residues 1 – 316), and SRF9 (residues 1 – 334) were amplified from *A. thaliana* cDNA, SOBIR1 (residues 1 - 270), PEPR (residues 1 - 767), FLS2 (residues 1 – 800), and EFR (residues 1 - 642) from *A. thaliana* genomic DNA. BAM1 (residues 20 – 637), and SERK5 (residues 24 - 214) were

synthesized (Geneart, Germany) with codons optimized for expression in *Trichoplusia ni*. The constructs were cloned in a modified pFastBac vector (Geneva Biotech) containing an azurocidin signal peptide, except for SERK2, SERK3, SRF3, SRF9, SOBIR1, PEPR, and FLS2 that were expressed using the native signal peptide, respectively, and a TEV (tabacco etch virus protease) cleavable C-terminal StrepII – 9x His tag. GSO1/SGN3 and GSO2 were also cloned into a vector harboring the *Drosophila* BiP secretion signal peptide, which was amplified from B02_SRF6_pECIA2 (2), a C-terminal TEV cleavable StrepII – 10x His tag and a non-cleavable Avi-tag (3, 4). GSO1/SGN3 variants carrying point mutations were generated using the primer extension method for site-directed mutagenesis. *Trichoplusia ni* (strain Tnao38) (5) cells were infected with a multiplicity of infection (MOI) of 1 at a density of 2 x 10^6 cells ml^{-1} and incubated for 26 h at 28 °C and for additional 48 h at 22 °C. The secreted protein was purified from the supernatant by Ni^{2+} (HisTrap Excel; GE healthcare; equilibrated in 50 mM KP_i pH 7.6, 250 mM NaCl, 1 mM 2-Mercaptoethanol) and StrepII (Strep-Tactin XT Superflow high affinity chromatography: IBA; equilibrated in 20 mM Tris pH 8.0, 250 mM NaCl, 1 mM EDTA) affinity chromatography. The tag was cleaved with His-tagged TEV protease at 4 °C overnight and removed by a second Ni^{2+} affinity chromatography step. Proteins were then further purified by size-exclusion chromatography on either a Superdex 200 increase 10/300 GL, Hi Load 16/600 Superdex 200 pg, or HiLoad 26/600 pg column (GE Healthcare), equilibrated in 20 mM sodium citrate pH 5.0, 250 mM NaCl. We purified ~5 mg GSO1/SGN3 and ~50 µg GSO2 from 8 L of insect cell culture, respectively. For crystallization, the GSO1/SGN3 ectodomain was dialyzed against 20 mM sodium citrate pH 5.0, 150 mM NaCl and treated with Endoglycosidase H, F1, and F3 to trim N-glycan chains, followed by size-exclusion chromatography to further purify the deglycosylated SGN3. His-tagged BirA was purified from *E. coli* by Ni^{2+} affinity chromatography.

Peptides

All peptides (see Supplementary table 2) were synthesized by Peptide Specialty Laboratories GmbH (Germany). The identify and integrity of each peptide was confirmed by mass spectrometry and all peptides, except for CIF4, were dissolved in water (CIF4 in 100% [v/v] DMSO), followed by dialysis in the respective buffer for the different analyses.

Isothermal titration calorimetry

All ITC experiments were perfomed on a MicroCal PEAQ-ITC (Malvern Panalytical) with a 200 µl sample cell and a 40 µl injection syringe at 25 °C. Proteins were dialyzed into ITC buffer (20 mM sodium citrate pH 5.0, 250 mM NaCl, exceptionally containing 5 % (v/v) DMSO for CIF4

experiments) prior to all titrations. A typical experiment consisted of injecting 200 µM CIF peptide in 2 µl intervals into the cell containing 20 µM GSO1/SGN3 receptor. The MicroCal PEAQ-ITC analysis software (version 1.21) was used for data analysis.

Right-angle light scattering

The oligmeric state of the recombiant GSO1/SGN3 ectodomain was analyzed by size exclusion chromatography coupled to right angle light scattering (SEC-RALS), using an OMNISEC RESOLVE / REVEAL combined system (Malvern Panalytical). Instrument calibration was performed with a BSA standard (Thermo Scientific Albumin Standard). 20 µM GSO1/SGN3 in the presence or absence of 100 µM CIF2, in a volume of 50 µl, were separated on a Superdex 200 increase 10/300 GL column (GE Healthcare) in 20 mM sodium citrate pH 5.0, 250 mM NaCl, at a column temperature of 35 °C and a flow rate of 0.7 ml min^{-1}. Data were analyzed using the OMNISEC software (version 10.41).

Biotinylation of proteins

The respective proteins (20 – 100 µM) were biotinylated with biotin ligase BirA (2 µM) (4) for 1 h at 25 °C, in a volume of 200 µl; 25 mM Tris pH 8, 150 mM NaCl, 5 mM MgCl2, 2 mM 2-Mercaptoethanol, 0.15 mM Biotin, 2 mM ATP, followed by size-exclusion chromatography to purify the biotinylated proteins.

Sulfotransferase assay

Sulfotransferase assays were performed with universal sulfotransferase activity kit (R&D systems, UK). Non-sulfated CIF2 (residues 59 – 72) (1 mM) were mixed with TPST using a 1:2 dilution series from 1 µM (48 ng $µl^{-1}$) in a volume of 50 µl; 50 mM Tris pH 7.5, 50 mM NaCl, 15 mM $MgCl_2$, 0.2 mM 3′-Phosphoadenosine 5′-phosphosulfate (PAPS), phosphatase (500 ng) for 30 min at 30 °C. 30 µl of malachite green reagent A and B, 100 µl of distilled water was added to each sample and incubated for 20 min at 30 °C. The absorption of each sample at 620 nm was determined with a microplate reader (Synergy2, Biotek). Phosphate standard curves were determined using a 1:2 dilution series starting from 100 mM KH_2PO_4. Product formation was calculated using the conversion factor from the phosphate standard curve.

Analytical size-exclusion chromatography

Gel filtration experiments were performed using a Superdex 200 Increase 10/300 GL column (GE Healthcare) equilibrated in 20 mM sodium citrate pH 5.0, 250 mM NaCl. A 500 µl aliquot of

GSO1/SGN3 and SERK1 or SERK3 (at a concentration of 10 µM) was loaded sequentially onto the column and elution at 0.75 ml min^{-1} was monitored by ultraviolet absorbance at 280 nm. The CIF2 peptide concentration was 20 µM in the GSO1/SGN3 – CIF2 – SERK1/SERK3 complex sample prior to loading.

Plant material and growth conditions

For all experiments, *Arabidopsis thaliana* (ecotype Columbia) was used. T-DNA tagged lines for *sgn3-3* (SALK_043282), *gso2* (SALK_143123C) and *cif3-2* (GABI_516E10) were obtained from NASC (http://arabidopsis.info/) and GABI (https://www.gabi-kat.de/) respectively. The *cif1-2 cif2-2* double mutant and *cif4* mutant were generated by CRISPR-Cas9 technique in Col wildtype or *cif3-2* mutant background (see below). Insertion points of the T-DNA and the CRISPR lines were verified by Sanger sequencing. Plants were grown on half-strength Murashige-Skoog (MS) agar (1%) for 5 d vertically after 2 d stratification at 4℃ in the dark. For peptide (Peptide Specialty Laboratories GmbH) treatment assays, seeds were germinated on medium with or without the indicated peptide concentrations and grown for 5d. Estradiol (Sigma) was dissolved in DMSO and used at 5 µM final concentration. DMSO concentration was 0.05% (v/v) at final dilution.

Molecular cloning

For promoter reporter lines, upstream regions of each gene - indicated by ‘length upstream of ATG’ - were cloned into gateway entry vectors and fused to NLS-3 x Venus via an LR reaction (pSGN3 5583 bp, pGSO2 3893 bp, pCIF1 1797 bp, pCIF2 1756 bp, pCIF3 2092 bp and pCIF4 2201bp). The pSGN3::SGN3-mVenus construct (1) was used as template to generate SGN3-mVenus variants by site-directed mutagenesis. CRISPR-Cas9 constructs were generated following a published method (6) after switching selection markers from Basta to FASTRed in the final construct with *S. pyogenes* Cas9. For generating *cif1-2* and *cif2-2*, 5’- ttgggtataagcttgaaagg -3’ and for generating *cif4-1* and *cif4-2*, 5’-aacccaagcccggtttacgg -3’ and 5’- ttggatttcaccctaaacga -3’ primers were used respectively. For constructing the dominant negative SERK3 (pSGN3::XVE>>SERK3(residues 1-243)-GFP), a fragment of SERK3 genomic region (residues 1-243.) was cloned into an entry vector and fused with pSGN3::XVE-LexA and GFP via a LR reaction. The constructs were transformed into the wild-type or *sgn3* mutant plants using the *Agrobacterium tumefaciens* GV3101 (MP90)-mediated floral dip method (7).

Microscopy

Signals were visualized using an SP8 microscope (Leica). Excitation and detection windows, respectively, were as follows: GFP (488 nm, 500-550 nm), Venus or mVenus (514 nm, 520 – 580 nm), propidium iodide (488 nm, 600 – 650 nm) and fuchsin (561 nm, 570 – 650 nm). Images were processed using the Fiji package of ImageJ (8).

Propidium iodide barrier assay

5d old seedlings were incubated in 10 µg/mL propidium iodide (PI) - water solution for 10 min and transferred into fresh water. For quantification, “onset of cell elongation” was defined as the point where endodermal cell length exceeded two times its width in a median longitudinal section. Cell counting was done using a Zeiss LSM 700 with a 488 nm laser and an SP640 filter split at 600 nm.

Toluidine blue staining

Sterilized seeds were sown on ½ MS plates and stratified for 2 d in the dark at 4 ℃. After stratification, seeds were transferred to a growth chamber and incubated for 6 h under continuous light followed by 4 and a half d in the dark. The seedlings were flooded with staining solution [0.05% (w/v) Toluidine Blue + 0.4% (v/v) Tween-20] for 2 minutes. Then the staining solution were removed and gently rinsed 3 times in water until the liquid is clear. Seedlings were photographed under a Zeiss AXIOZoom microscope.

Visualization of lignin

Lignin staining was performed as described in previous reports (9, 10). Briefly, 5 d old seedlings were fixed in 4% (v/v) paraformaldehyde PBS solution (pH 6.9) for 1 h without vacuum treatment. The samples were rinsed with PBS twice and incubated in ClearSee (10% (w/v) xylitol, 15% (w/v) sodium deoxycholate, 25% (w/v) urea in water) solution overnight. After removing the solution, samples were stained with 0.2% fuchsin in ClearSee solution overnight. Fuchsin solution was removed and the seedlings were briefly rinsed with fresh ClearSee solution and washed by gently agitation in fresh ClearSee solution for 30 min. After exchanging the ClearSee solution, the seedlings were washed overnight.

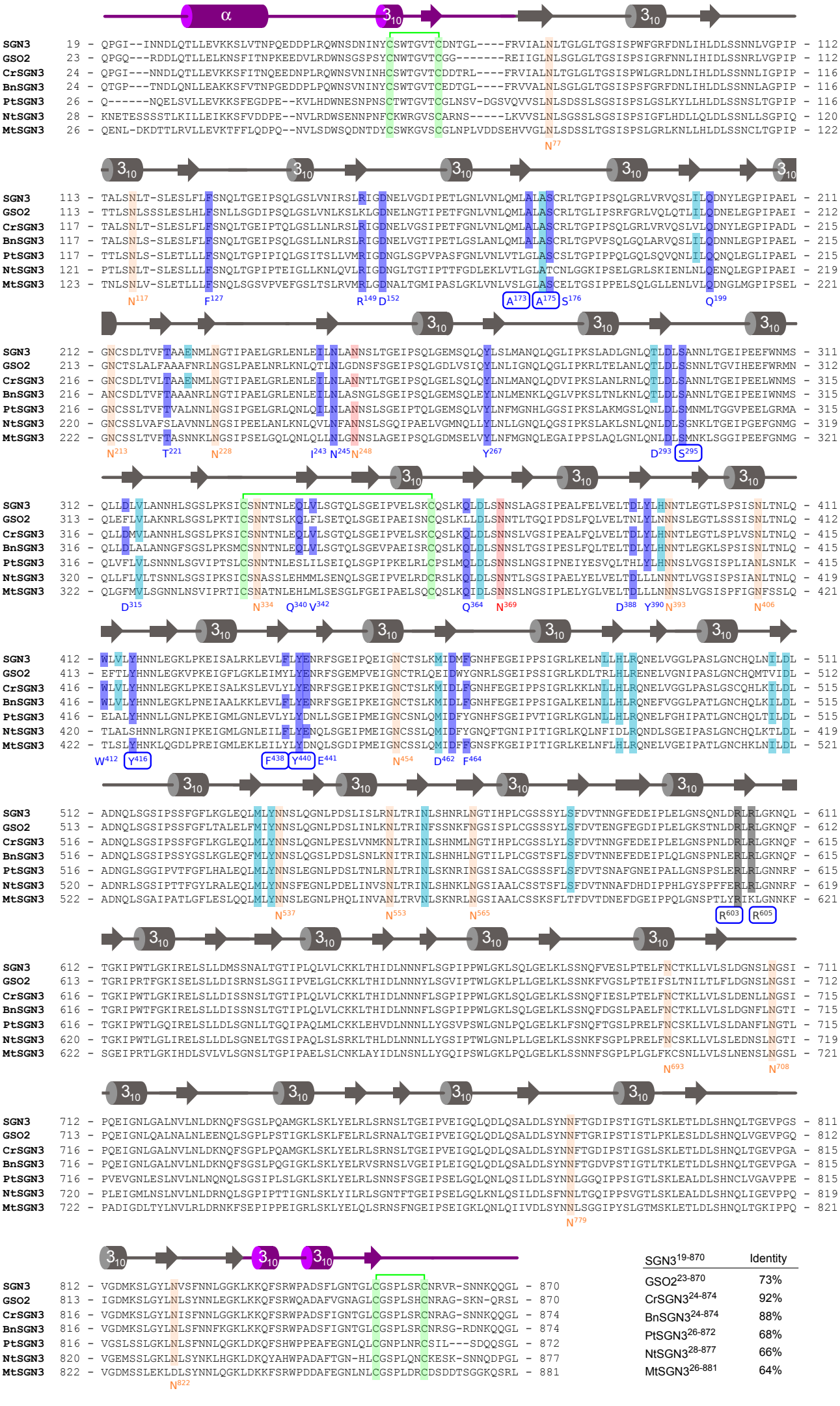

SGN3[19-870]	Identity
GSO2[23-870]	73%
CrSGN3[24-874]	92%
BnSGN3[24-874]	88%
PtSGN3[26-872]	68%
NtSGN3[28-877]	66%
MtSGN3[26-881]	64%

Fig. S1 Structure-based multiple sequences alignment of SGN3 ectodomains from *Arabidopsis thaniana* GSO1/SGN3 (NCBI (https://www.ncbi.nlm.nih.gov/) identifier: OAO97463), GSO2 (NCBI identifier: OAO90459), *Capsella rubella* SGN3 (NCBI identifier: XP_006285037.2), *Brassica napus* SGN3 (NCBI identifier: XP_013660918.1), *Populus trichocarpa* SGN3 (NCBI identifier: XP_002299384.1), *Nicotiana tabacum* SGN3 (NCBI identifier: XP_016509707.1), and *Medicago truncatula* SGN3 (NCBI identifier: XP_013457406.1). A secondary structure assignment, calculated with DSSP (11), is shown beside. SGN3 residues forming hydrogen bonds with CIF2 in the SGN3 – CIF2 complex are highlighted in blue, residues interacting with CIF2 in cyan, glycosylated asparagine residues in orange, asparagine residues with glycans directly contacted with CIF2 in red, the RxR motif in gray, and cysteines forming disulfide bonds in light green. All numbering refers to AtGSO1/SGN3. Table summarizes amino acid sequence identities among SGN3 ectodomains versus AtSGN3.

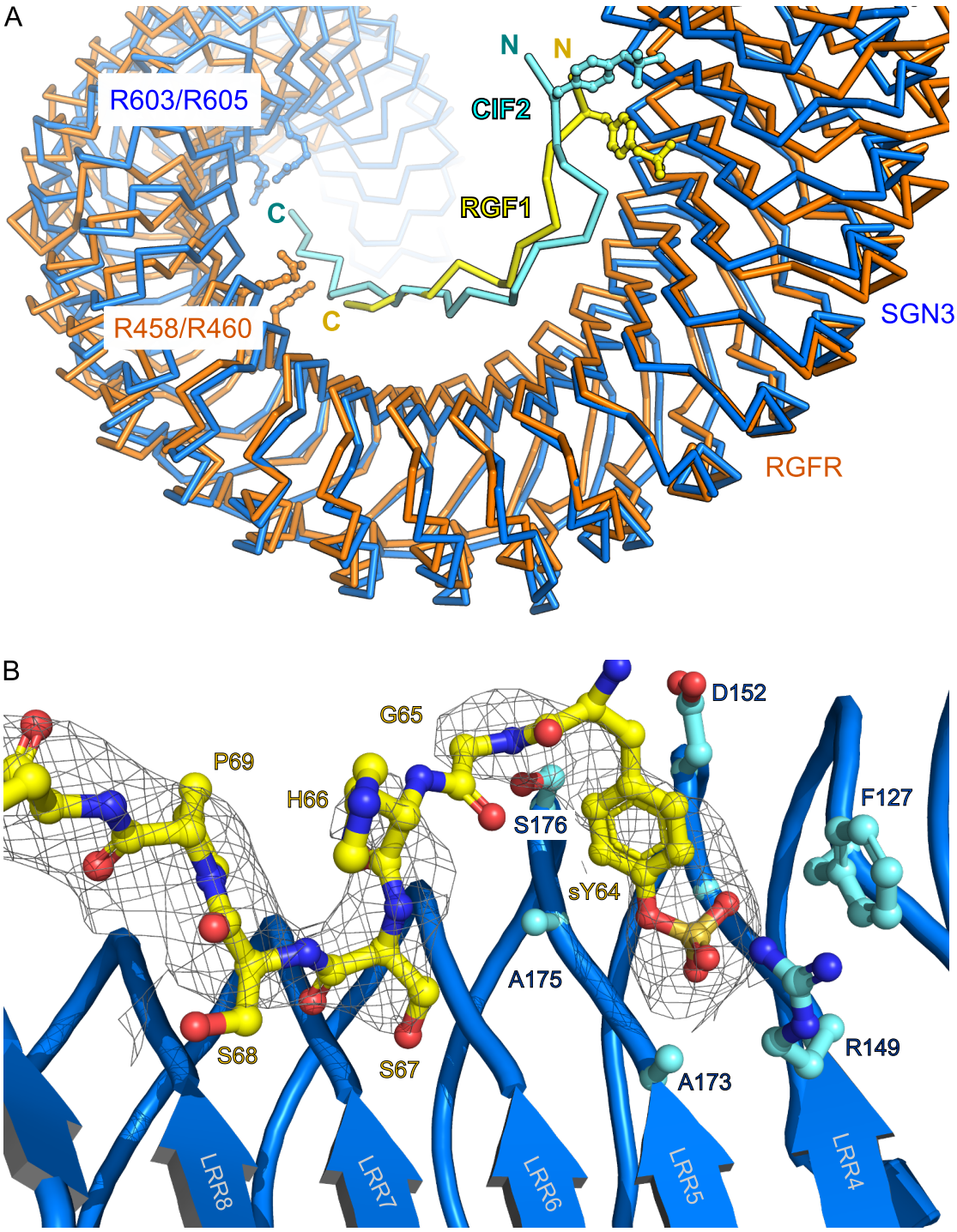

Fig. S2. Different LRR-RKs binding tyrosine sulfated peptide share structural similarity.
(*A*) Structural superposition of GSO1/SGN3 – CIF2 (blue and cyan C_α traces, respectively) and RGFR – RGF1 (orange and yellow; PDB ID 5hyx) complex structures. The conserved arginine residues of the RxR motif are shown. The two complex structures align with a root mean square displacement (r.m.s.d.) of ~ 3.1 Å comparing 498 corresponding C_α atoms. (*B*) Details of the sTyr binding pocket in GSO1/SGN3 (blue ribbon diagram). The synthetic sTyr-containing CIF2 peptide is shown in bonds representation (in yellow) and including a $2F_o$-F_c omit electron density map contoured at 1.5 σ. Residues contributing to the sTyr binding pocket in GSO1/SGN3 are included (in bonds representation).

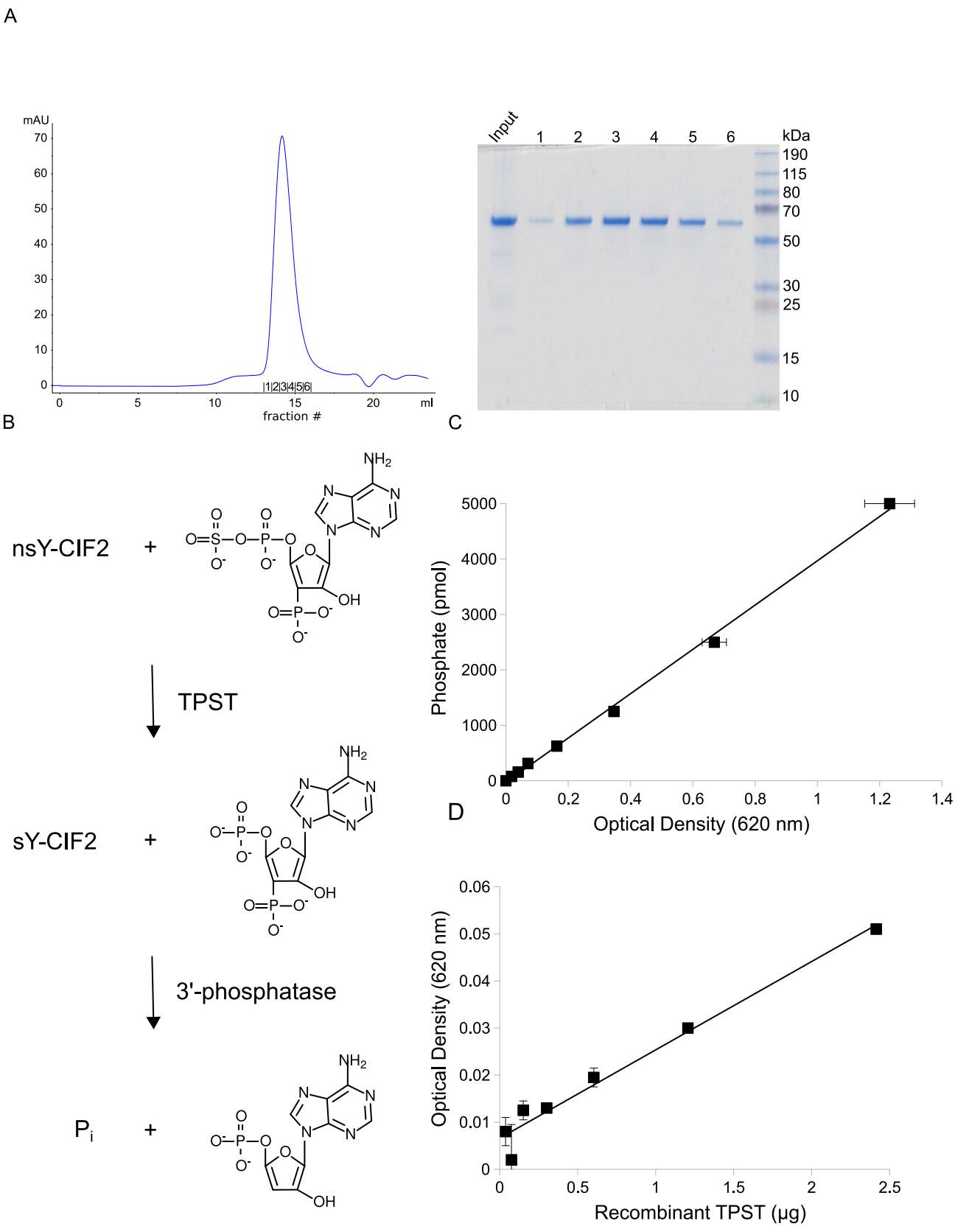

Fig. S3. CIF2 is a substrate of the plant tyrosylprotein sulfotransferase TPST/SGN2. (*A*) Size-exclusion chromatography trace of TPST (residues 25 – 441) purified from insect cells. (*Right*) Coomassie-stained SDS PAGE of the corresponding elution fractions. (*B*) Schematic overview of the sulfotransferase assay. Inorganic phosphate (Pi) release was detected using a malachite green Pi quantification assay to derive the enzyme kinetics of the sufotransferase reaction. (*C*) Pi standard curve used for the enzymatic assay. (*D*) 0.2 mM 3′-Phosphoadenosine 5′-phosphosulfate (PAPS) was incubated with varying concentrations of TPST for 30 min at 30 °C. Optical densities (ODs) were plotted versus the amount of TPST recombinant protein. A specific activity of 1.25 pmol min^{-1} $µg^{-1}$ was calculated.

A

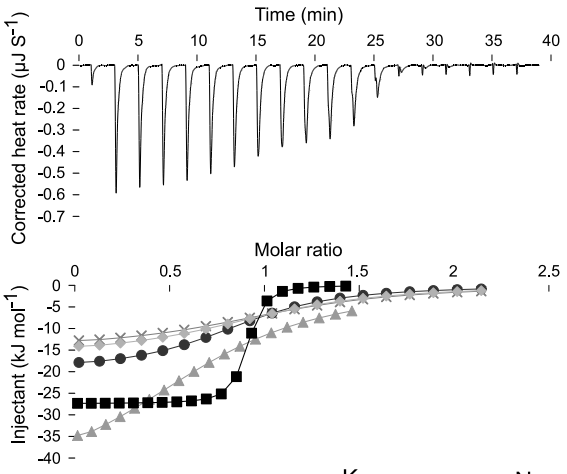

		K_d	N
■	CIF2^{WT} vs SGN3 ^{WT}	9.0 ± 5.6 nM	0.877 ± 0.003
◆	CIF2^{nsY64} vs SGN3^{WT}	3.0 ± 0.3 µM	1.00 ± 0.016
▲	CIF2^{Y64F} vs SGN3^{WT}	5.0 ± 2.5 µM	0.755 ± 0.077
●	CIF2^{WT} vs SGN3^{A173Q,A175Q}	1.9 ± 0.1 µM	0.874 ± 0.008
×	CIF2^{nsY64} vs SGN3^{A173Q,A175Q}	3.3 ± 0.3 µM	1.085 ± 0.018

ITC experiments

peptide ligand	receptor ectodomain	K_d (ITC)	Additive
CIF2^{WT}	SGN3^{WT}	9.0 nM	
CIF2^{nsY64}	SGN3^{WT}	3.0 µM	
CIF2^{Y64F}	SGN3^{WT}	2.4 µM	
CIF^{L80D}	SGN3^{WT}	146 nM	
CIF2^{I81D}	SGN3^{WT}	71.2 nM	
CIF1$^{Hyp69, Hyp71}$	SGN3^{WT}	43.2 nM	
CIF2^{WT}	SGN3^{WT}	261 nM	+DMSO
CIF4	SGN3^{WT}	300 nM	+DMSO
CIF2^{WT}	SGN3$^{A173Q, A175Q}$	1.7 µM	+DMSO
CIF2^{nsY64}	SGN3^{WT}	6.4 µM	+DMSO

C

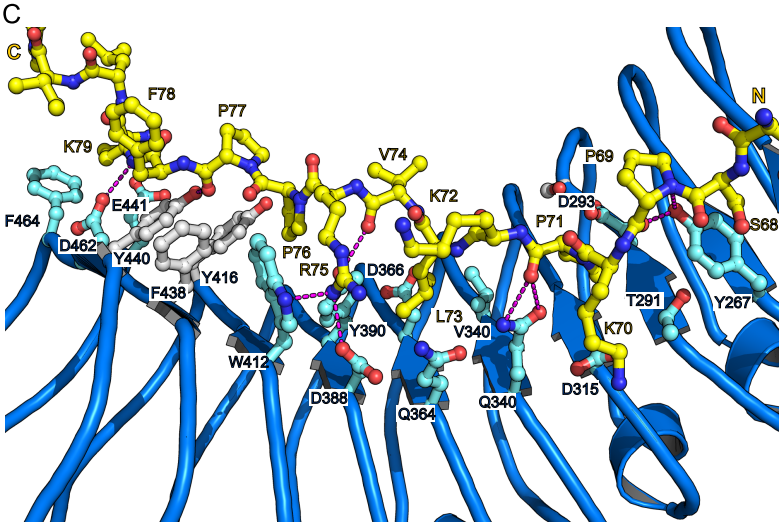

B

GCI experiments

peptide ligand	receptor ectodomain	K_d (GCI)
CIF2^{WT}	SGN3^{WT}	0.9 nM
CIF2$^{Hyp69, Hyp71}$	SGN3^{WT}	1.9 nM
CIF2^{nsY64}	SGN3^{WT}	1.2 µM
CIF1^{WT}	SGN3^{WT}	4.9 nM
CIF1$^{Hyp69, Hyp71}$	SGN3^{WT}	6.1 nM
CIF3^{WT}	SGN3^{WT}	3.8 nM
CIF3^{nsY46}	SGN3^{WT}	184 nM
CIF2^{WT}	SGN3$^{R603A, R605A}$	9.5 nM
CIF2^{nsY64}	SGN3$^{R603A, R605A}$	n.d.
CIF1^{WT}	SGN3$^{R603A, R605A}$	6.0 nM
CIF3^{WT}	SGN3$^{R603A, R605A}$	2.4 nM
CIF3^{nsY46}	SGN3$^{R603A, R605A}$	75 nM
CIF2^{WT}	SGN3^{R605A}	3.3 nM
CIF2^{nsY64}	SGN3^{R605A}	2.8 µM
CIF1^{WT}	SGN3^{R605A}	6.1 nM
CIF3^{WT}	SGN3^{R605A}	4.7 nM
CIF3^{nsY46}	SGN3^{R605A}	230 nM
CIF2^{WT}	SGN3^{R603A}	6.8 nM
CIF2^{nsY64}	SGN3^{R603A}	n.d.
CIF1^{WT}	SGN3^{R603A}	4.5 nM
CIF2^{WT}	SGN3$^{A173Q, A175Q}$	n.d.
CIF2^{nsY64}	SGN3$^{A173Q, A175Q}$	n.d.
CIF1^{WT}	SGN3$^{A173Q, A175Q}$	n.d.
CIF3^{WT}	SGN3$^{A173Q, A175Q}$	n.d.
CIF3^{nsY46}	SGN3$^{A173Q, A175Q}$	n.d.
CIF2^{WT}	SGN3^{A173Q}	n.d.
CIF2^{nsY64}	SGN3^{A173Q}	n.d.
CIF1^{WT}	SGN3^{A173Q}	n.d.
CIF3^{WT}	SGN3^{A173Q}	n.d.
CIF3^{nsY46}	SGN3^{A173Q}	n.d.
CIF2^{WT}	SGN3^{A175Q}	n.d.
CIF2^{nsY64}	SGN3^{A175Q}	n.d.
CIF1^{WT}	SGN3^{A175Q}	n.d.
CIF3^{WT}	SGN3^{A175Q}	n.d.
CIF3^{nsY46}	SGN3^{A175Q}	n.d.
CIF2^{WT}	SGN3$^{3x mut}$	16 nM
CIF2^{nsY64}	SGN3$^{3x mut}$	14 µM
CIF2^{WT}	SGN3$^{6x mut}$	n.d.
CIF2^{nsY64}	SGN3$^{6x mut}$	n.d.
CIF2^{WT}	GSO2	n.d.
CIF1^{WT}	GSO2	n.d.
CIF3^{WT}	GSO2	3.9 nM

Fig. S4. Mutational characterization of the GSO1/SGN3 – CIF2 complex interface.
(*A*) Isothermal titration calorimetry (ITC) assays of CIF2 variants versus GSO1/SGN3 wild-type and mutant ectodomains. Table summaries for dissociation constants (K*d*) and binding stoichiometries (N) are shown (± fitting error). (*B*) GCI assays of CIF variants versus GSO1/SGN3 wild-type and mutant ectodomains. Peptides were supplied at a flow rate of 100 µl min^{-1}. Binding kinetics were analyzed using a one-to-one binding model. Table summaries of kinetic parameters are shown (D_c/D_i, density of captured/immobilized protein; k_{on}, association rate constant; k_{off}, dissociation rate constant; K_d, dissociation constant; n.d., no detectable binding). (*C*) Details of the interactions of the CIF2 central part with GSO1/SGN3 LRRs 6–17. Interface residues are shown in bonds representation, hydrogen bonds as dotted lines (in magenta). Amino-acids targeted for mutational analysis are shown in gray.

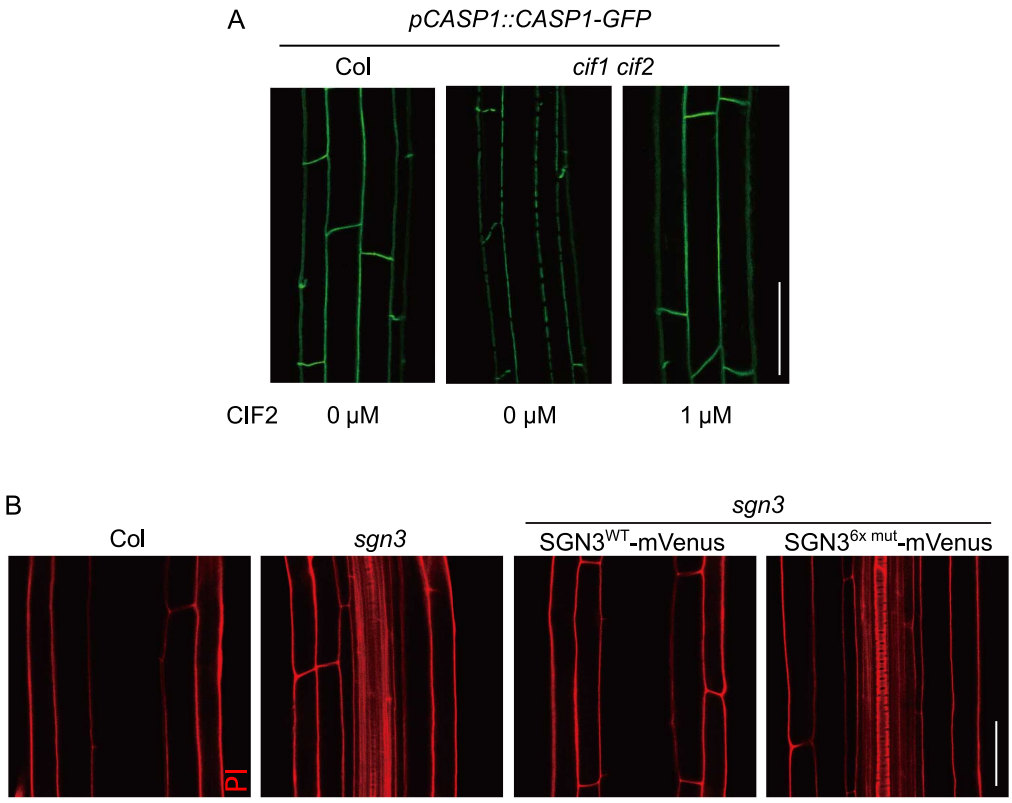

Fig. S5. The GSO1/SGN3$^{6x\ mut}$ sixtuple mutant fails to complement the *sgn3* Casparian strip phenotype.
(*A*) Casparian strip domains are visualized in Col (WT) and *cif1 cif2* in the pre- or absence of CIF2 at the indicated concentration. Scale bar = 20 µm (*B*) Representative images of PI permeability in roots of the indicated genotypes. Pictures were taken around 25-30 cells after onset of endodermal cell elongation. *sgn3* and *sgn3* transformed with GSO1/SGN3$^{6x\ mut}$-mVenus both display staining of vasculature, which is indicative of barrier defect. Scale bar = 40 µm.

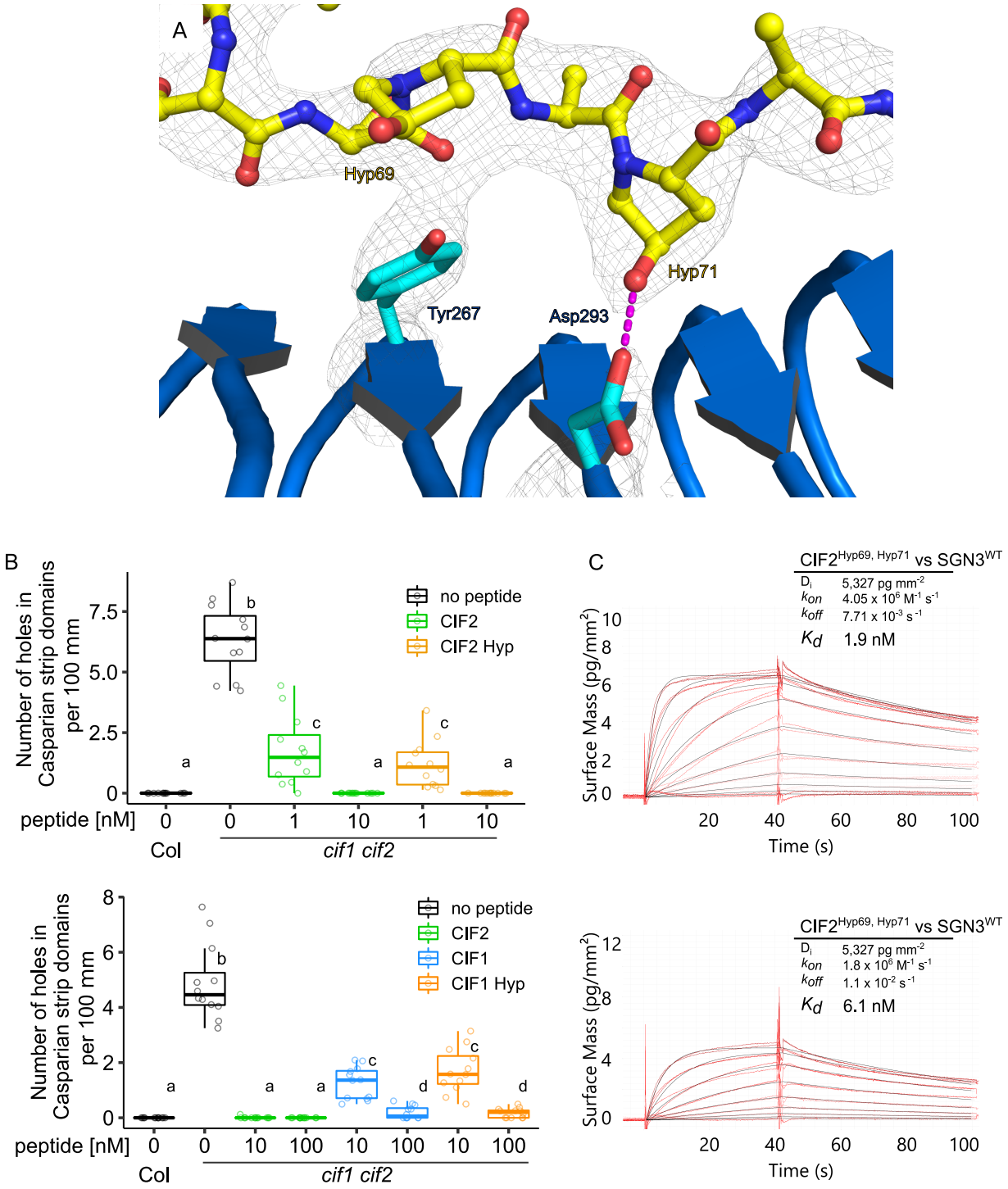

Fig. S6. Two hydroxylprolines in CIF2 are dispensable for GSO1/SGN3 binding. (*A*) Details of the interaction between two hydroxyproline residues of $CF2^{Hyp69, 71}$ (yellow, in bonds representation) and the SGN3 ectodomain (blue ribbon diagram). Hydrogen bonds are depicted as dotted lines (in magenta), a $2F_o$-F_c omit electron density map contoured at 1.5 σ is shown alongside (gray mesh). (*B*) Quantitative analyses of number of holes in Casparian strip domains per 100 µm in *cif1 cif2* double mutants treated with CIF peptide-variants (n=12 for each condition). Shown are box plots spanning the first to third quartiles, with the bold line representing the median, and circles indicating the raw data. Wiskers indicate maximum and minimum values, except outliers. The different letters indicate statistically significant differences (b, c, statistically significant difference with $p < 0.05$, one-way ANOVA and Tukey test) (*C*) GCI assays of hydroxyprolinated CIF variants versus the SGN3 wild type ectodomain. The flow rate was 100 µl min^{-1} for all experiments. Sensorgrams are shown with raw data in red and their respective fits in black. A one-to-one binding model was used, table summaries of kinetic parameters are shown alongside (D_i, density of immobilized protein; k_{on}, association rate constant; k_{off}, dissociation rate constant; K_d, dissociation constant).

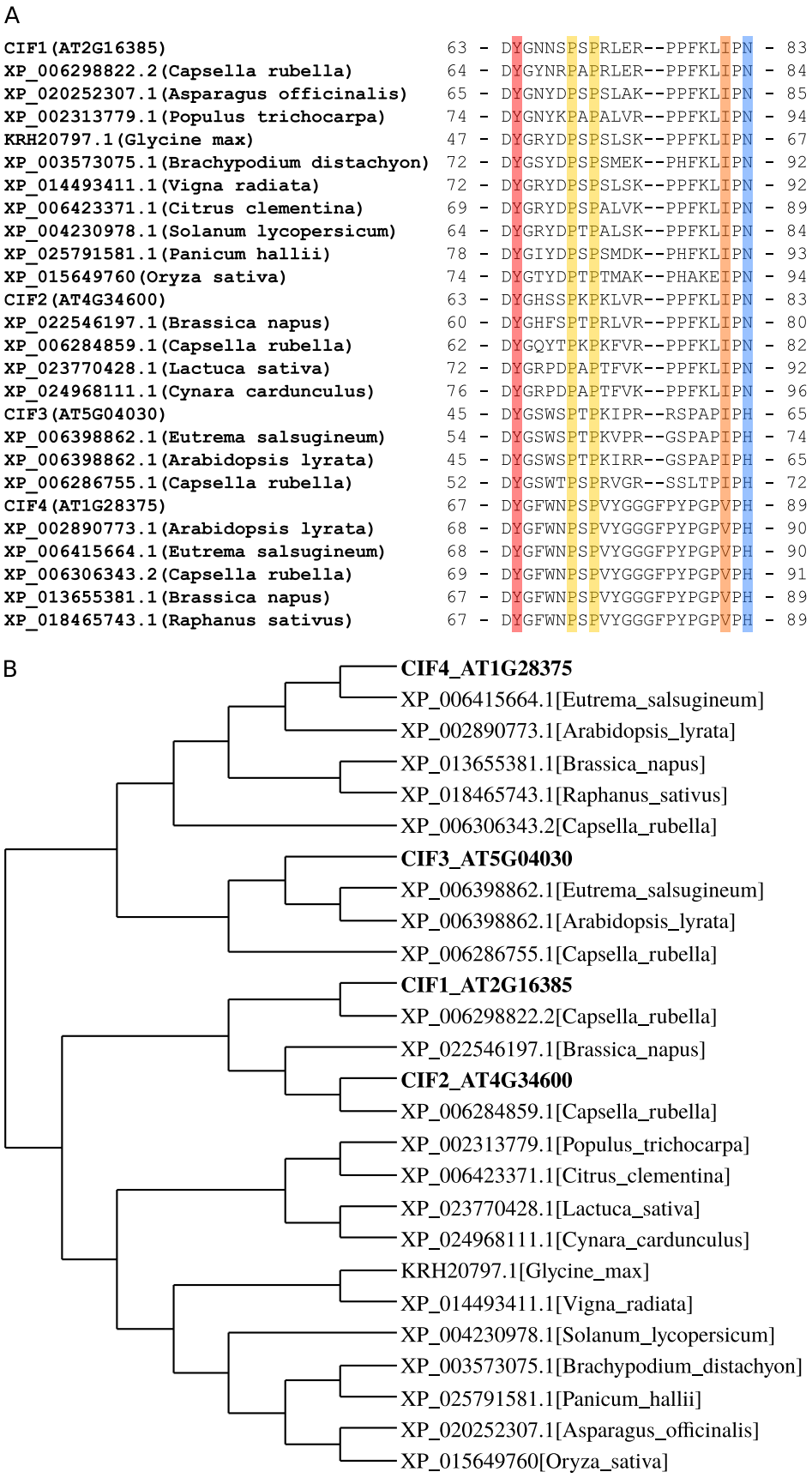

Fig. S7. CIF3 and CIF4 orthologs are present in other plant species. (*A*) Multiple sequence alignment of CIF1-4 from *Arabidopsis thaliana* and their putative orthologs from other plant species. Sequences were obtained from NCBI (https://www.ncbi.nlm.nih.gov/) and aligned with the program T-coffee (version 12.0) (12). The conserved sulfated tyrosine is highlighted in red, hydroxyprolines in yellow, the conserved isoleucine in orange, and the C-terminal asparagine or histidine residue in blue. (*B*) Phylogenetic tree of CIF peptides prepared with the program BIONJ (13).

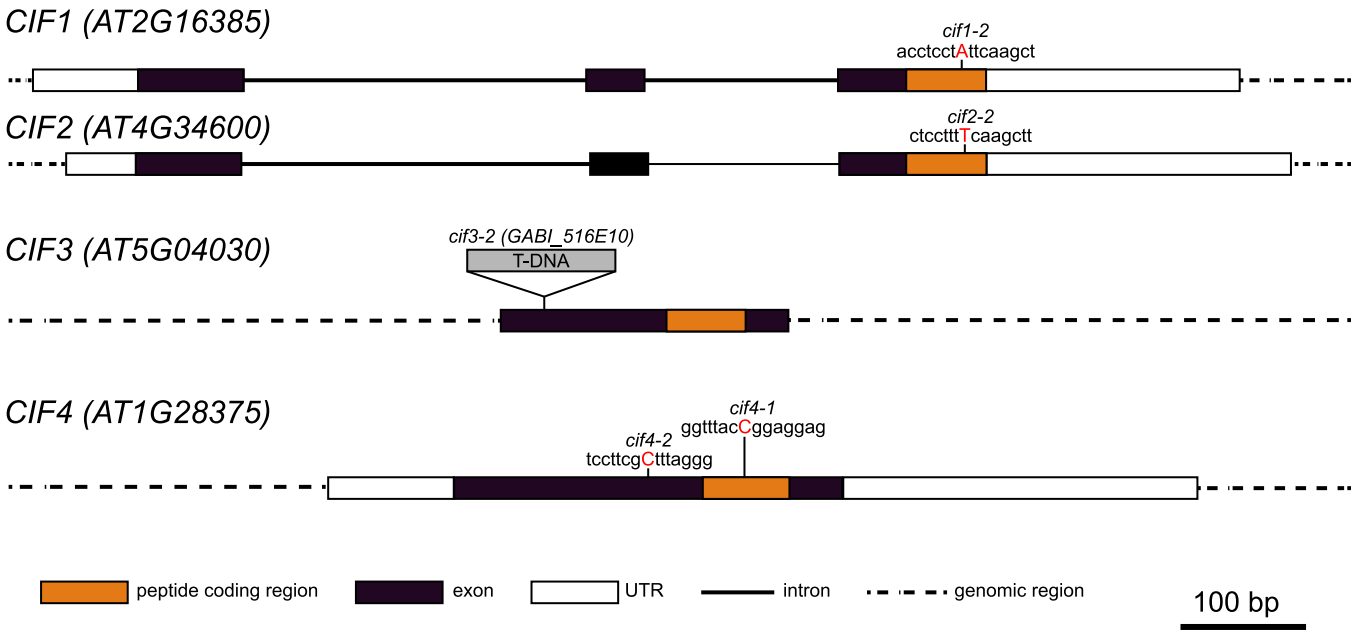

Fig. S8. Overview of the CIF mutant alleles used in this study.
Schematic CIF gene models and their respective mutant alleles. Single base pair insertion points (indicated by red uppercase letters) are shown with neighboring sequences. The T-DNA insertion point is indicated in the CIF3 locus by a gray box.

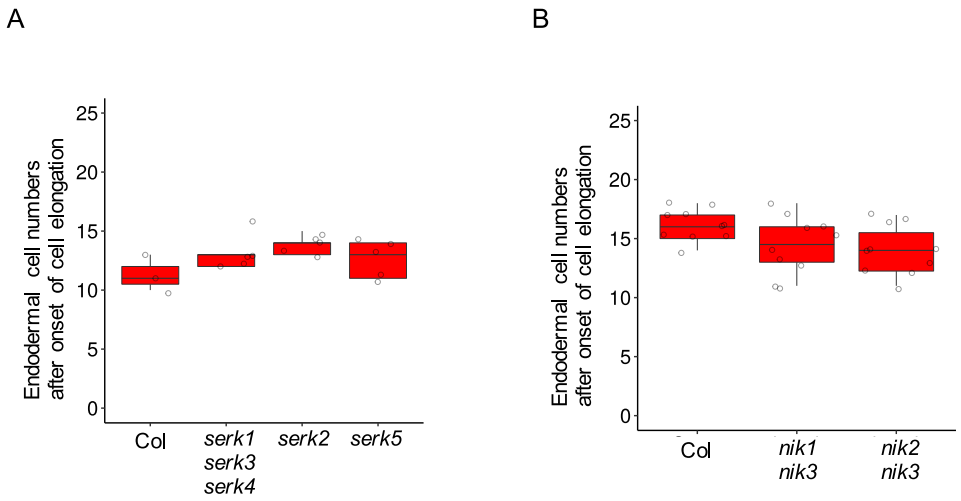

Fig. S9. Different *serk* and *nik* co-receptor loss-of-function mutants display no apparent Casparian strip defects.
PI penetration assay with several *serk* and *nik single and/or multiple* mutants. Barrier function was scored by counting the cell numbers until PI became impermeable to the steles. Shown are box plots spanning the first to third quartiles, with the bold line representing the median, and circles indicating the raw data. Wiskers indicate maximum and minimum values, except outliers.

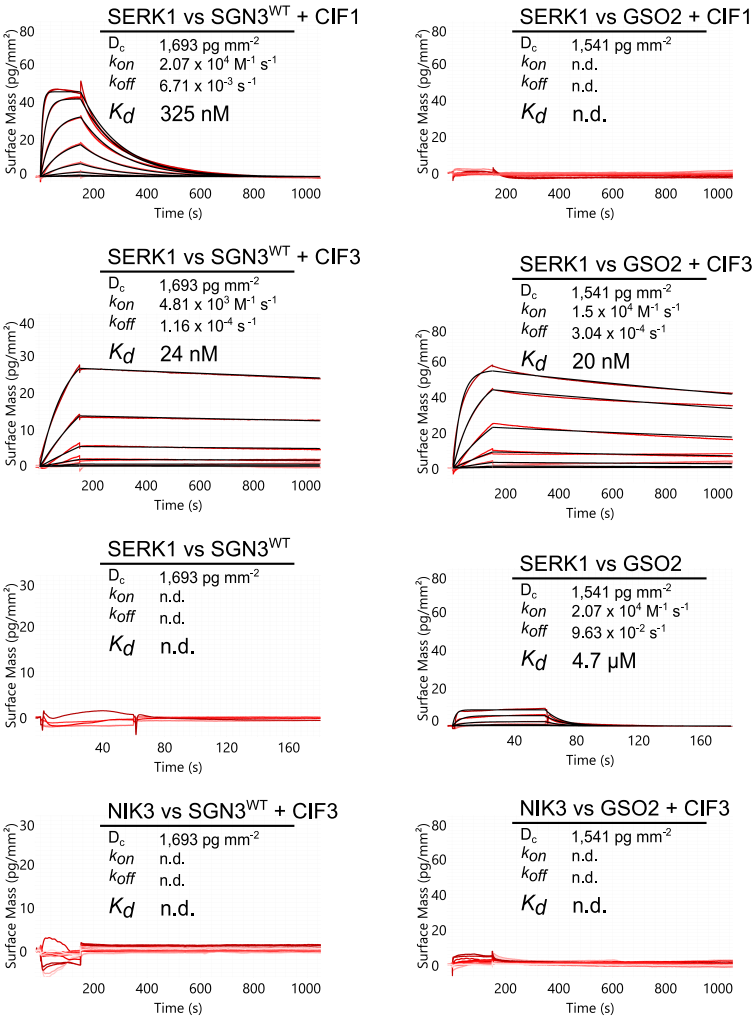

co-receptor	receptor	peptide	K_d
SERK1	SGN3 ^{WT}	CIF1	325 nM
SERK1	SGN3 ^{WT}	CIF2^{WT}	265 nM
SERK1	SGN3 ^{WT}	CIF3	24 nM
SERK1	SGN3 ^{WT}	-	n.d.
SERK1	SGN3 ^{WT}	CIF2^{I81D}	n.d.
SERK1	SGN3 $^{6x\ mut}$	CIF1	n.d.
SERK1	SGN3 $^{6x\ mut}$	CIF2^{WT}	n.d.
SERK1	SGN3 $^{6x\ mut}$	CIF3	n.d.
SERK1	GSO2	CIF1	n.d.
SERK1	GSO2	CIF2^{WT}	n.d.
SERK1	GSO2	CIF3	20 nM
SERK1	GSO2	-	4.7 µM
SERK3	SGN3 ^{WT}	CIF3	89 nM
SERK3	SGN3 $^{6x\ mut}$	CIF3	n.d.
SERK3	GSO2	CIF3	49 nM
SERK5	SGN3 ^{WT}	CIF3	n.d.
SERK5	GSO2	CIF3	n.d.
NIK3	SGN3 ^{WT}	CIF3	n.d.
NIK3	GSO2	CIF3	n.d.
NIK4	SGN3 ^{WT}	CIF3	n.d.
NIK4	GSO2	CIF3	n.d.
SRF3	SGN3 ^{WT}	CIF3	n.d.
SRF3	GSO2	CIF3	n.d.
SRF9	SGN3 ^{WT}	CIF3	n.d.
SRF9	GSO2	CIF3	n.d.
SOBIR1	SGN3 ^{WT}	CIF3	n.d.
SOBIR1	GSO2	CIF3	n.d.

Fig. S10. GSO1/SGN3 and GSO2 bind SERK1 and SERK3 co-receptor kinases in the presence of CIF peptides. GCI assays of co-receptor candidates versus GSO1/SGN3 and GSO2 ectodomains in the presence of CIF peptides. Co-receptor candidates were applied at a flow rate of 25 µl min^{-1}. Sensorgrams are shown with raw data in red and their respective fits in black. Binding kinetics were analyzed using a one-to-one binding model. Table summaries of kinetic parameters are shown (D_c, density of captured protein; k_{on}, association rate constant; k_{off}, dissociation rate constant; K_d, dissociation constant; n.d., no detectable binding).

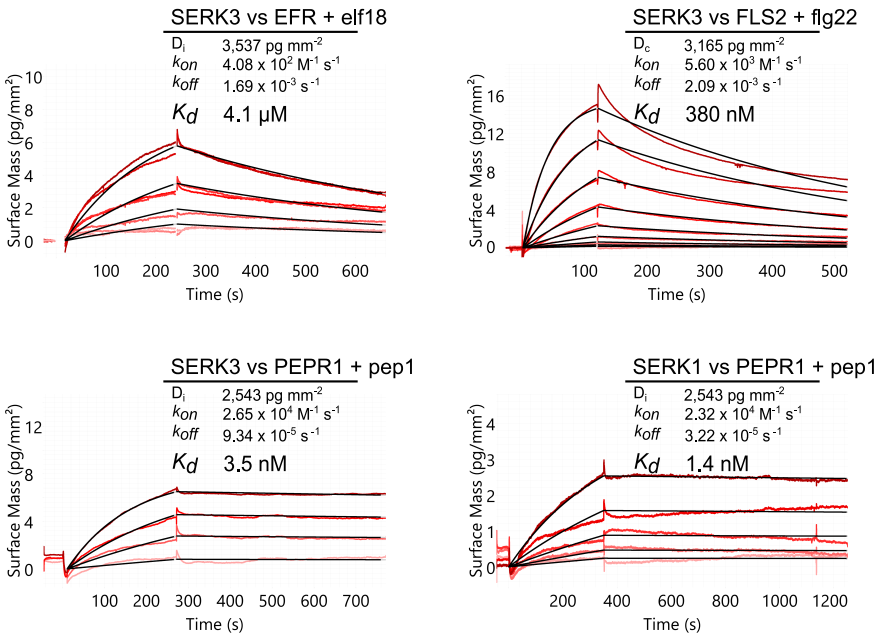

Fig. S11. The LRR-RKs EFR, FLS2 and PEPR1 bind SERKs with very different binding affinities and -kinetics. GCI assays of co-receptors versus cognate LRR-RKs in the presence of peptide ligands. The flow rate was adjusted to 50 µl min^{-1} for EFR, 20 µl min^{-1} for FLS2, and 35 µl min^{-1} for PEPR1, respectively. Sensorgrams are shown with raw data in red and their respective fits in black. A one-to-one binding model was used, table summaries of kinetic parameters are shown (D_c/D_i, density of captured/immobilized protein; k_{on}, association rate constant; k_{off}, dissociation rate constant; K_d, dissociation constant).

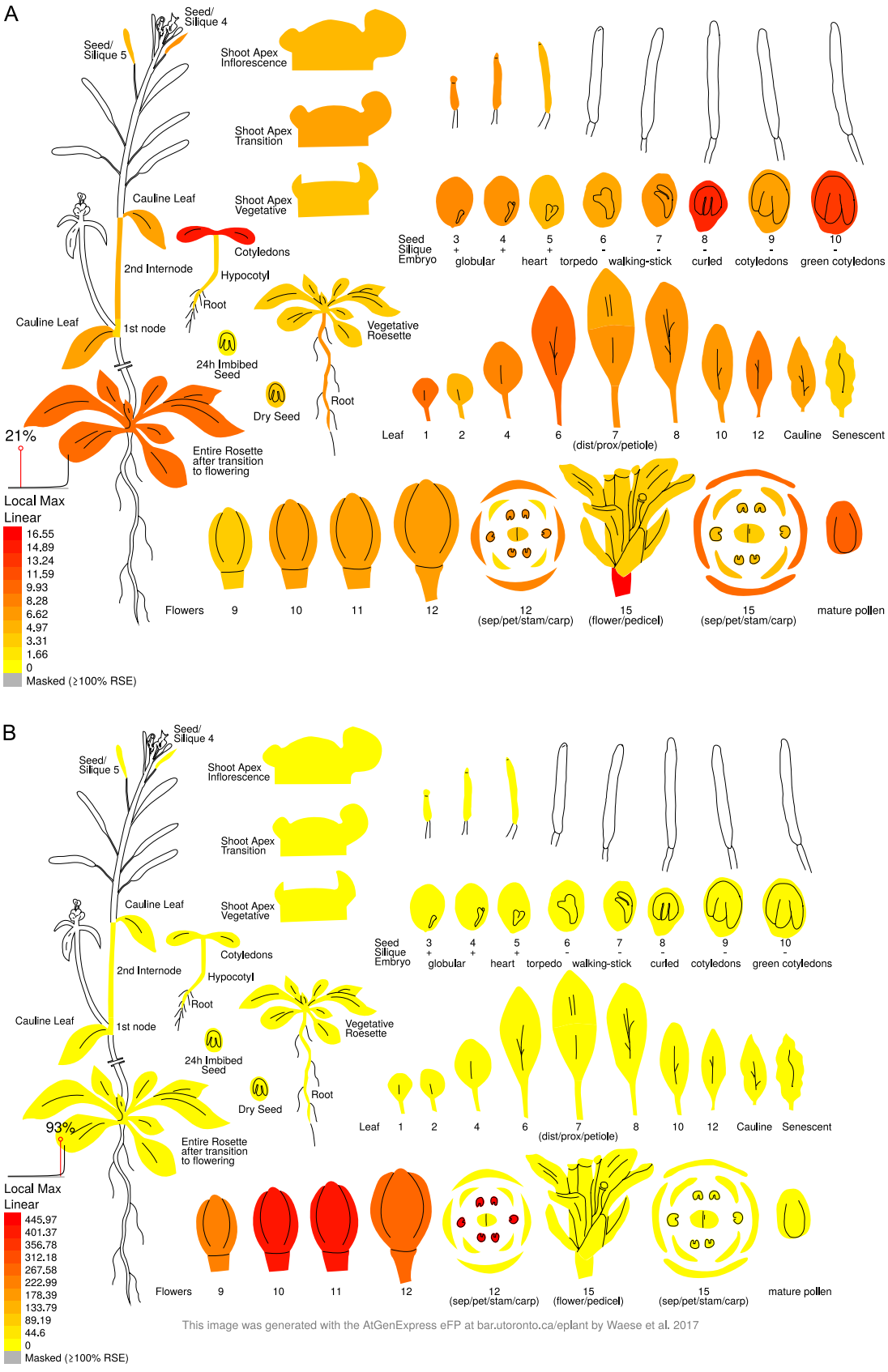

Fig. S12 Expression analysis suggests putative functions for CIF3 and CIF4 outside the Casparian strip. Expression-pattern images of CIF3 (*A*) and CIF4 (*B*) were generated with the AtGenExpress eFP (https://bar.utoronto.ca/eplant/, (14)) using publically available microarray data (16, 17). CIF3 appears to be expressed at embryo stage and in cotyledons, while CIF4 shows strong expression in early stage flowers and in stamens.

Supplementary Tables

Table S1. Crystallographic data collection and refinement

	GSO1/SGN3 – CIF2	**GSO1/SGN3 - CIF2**
	sulfur SAD	*native*
Data collection		
Space group	$P4_32_12$	$P4_32_12$
Wavelength (Å)	2.066403	1.000006
Cell dimensions		
a, *b*, *c* (Å)	192.1, 192.1, 149.3	192.4, 192.4, 149.8
α, β, γ (°)	90, 90, 90	90, 90, 90
Resolution (Å)	48.75 – 4.00 (4.10 – 4.00)	48.32 – 2.95 (3.03 – 2.95)
R_{meas} [#]	0.247 (0.80)	0.237 (4.54)
CC(1/2) *(%)*[#]	99.9 (96.5)	100.0 (47.7)
$I/\sigma I$[#]	15.6 (5.0)	19.1 (0.9)
Completeness (%)[#]	99.9 (99.9)	100.0 (100.0)
Redundancy[#]	27.6 (27.1)	40.1 (42.2)
Wilson B-factor[#]		84.1
Refinement		
Resolution (Å)		48.32 – 2.95
No. reflections		59,498
R_{work}/ R_{free} [$]		0.21/0.28
No. atoms		
protein		12,732
CIF peptide		348
glycan		495
Res. B-factors[$]		
protein		102.2
CIF peptide		117.1
glycan		128.7
R.m.s deviations[$]		
Bond lengths (Å)		0.0125
Bond angles (°)		1.64
Molprobity results		
Ramachandran outliers (%)[‡]		0.18
Ramachandran favored (%)[‡]		91.75
Molprobity score[‡]		2.17
PDB - ID		**6S6Q**

[#] as implemented in XDS (16)
[$] as implemented in phenix.refine (17)
[‡] as implemented in phenix.molprobity (18)

Table S2. Amino acid sequences of synthesized peptides

Peptide	Sequence
CIF1^{WT}	D(sY)GNNSPSPRLERPPFKLIPN
CIF2^{WT}	D(sY)GHSSPKPKLVRPPFKLIPN
CIF3^{WT}	D(sY)GSWSPTPKIPRRSPAPIPH
CIF4	D(sY)GFWNPSPVYGGGFPYPGPVPH
CIF2$^{59-72}$	MNSRDYGHSSPKPK
CIF2^{nsY64}	DYGHSSPKPKLVRPPFKLIPN
CIF3^{nsY46}	DYGSWSPTPKIPRRSPAPIPH
CIF2^{Y64F}	DFGHSSPKPKLVRPPFKLIPN
CIF2$^{Hyp69, Hyp71}$	D(sY)GHSS(HyP)K(HyP)KLVRPPFKLIPN
CIF1$^{Hyp69, Hyp71}$	D(sY)GNNS(HyP)S(HyP)RLERPPFKLIPN
CIF2^{L80D}	D(sY)GHSSPKPKLVRPPFKDIPN
CIF2^{I81D}	D(sY)GHSSPKPKLVRPPFKLDPN
Pep1	ATKVKAKQRGKEKVSSGRPGQHN
Pep2	DNKAKSKKRDKEKPSSGRPGQTNSVPNAAIQVYKED
CLE9	RLV(HyP)SG(HyP)NPLHN
flg22	QRLSTGSRINSAKDDAAGLQIA
elf18	SKEKFERTKPHVNVGTIG

sY, sulfated tyrosine
HyP, Hydroxyproline

Supplementary references

1. A. Pfister, *et al.*, A receptor-like kinase mutant with absent endodermal diffusion barrier displays selective nutrient homeostasis defects. *eLife* **3**, e03115 (2014).
2. E. Smakowska-Luzan, *et al.*, An extracellular network of Arabidopsis leucine-rich repeat receptor kinases. *Nature* **553**, 342–346 (2018).
3. M. G. Cull, P. J. Schatz, "Biotinylation of proteins in vivo and in vitro using small peptide tags" in *Methods in Enzymology*, Applications of Chimeric Genes and Hybrid Proteins Part A: Gene Expression and Protein Purification., (Academic Press, 2000), pp. 430–440.
4. M. Fairhead, M. Howarth, "Site-Specific Biotinylation of Purified Proteins Using BirA" in *Site-Specific Protein Labeling: Methods and Protocols*, Methods in Molecular Biology., A. Gautier, M. J. Hinner, Eds. (Springer New York, 2015), pp. 171–184.
5. Y. Hashimoto, S. Zhang, G. W. Blissard, Ao38, a new cell line from eggs of the black witch moth, Ascalapha odorata (Lepidoptera: Noctuidae), is permissive for AcMNPV infection and produces high levels of recombinant proteins. *BMC Biotechnol.* **10**, 50 (2010).
6. F. Fauser, S. Schiml, H. Puchta, Both CRISPR/Cas-based nucleases and nickases can be used efficiently for genome engineering in Arabidopsis thaliana. *Plant J.* **79**, 348–359 (2014).
7. S. J. Clough, A. F. Bent, Floral dip: a simplified method forAgrobacterium-mediated transformation ofArabidopsis thaliana. *Plant J.* **16**, 735–743 (1998).
8. J. Schindelin, *et al.*, Fiji: an open-source platform for biological-image analysis. *Nat. Methods* **9**, 676–682 (2012).
9. D. Kurihara, Y. Mizuta, Y. Sato, T. Higashiyama, ClearSee: a rapid optical clearing reagent for whole-plant fluorescence imaging. *Development* **142**, 4168–4179 (2015).
10. R. Ursache, T. G. Andersen, P. Marhavý, N. Geldner, A protocol for combining fluorescent proteins with histological stains for diverse cell wall components. *Plant J.* **93**, 399–412 (2018).
11. C. Notredame, D. G. Higgins, J. Heringa, T-coffee: a novel method for fast and accurate multiple sequence alignment1. *J. Mol. Biol.* **302**, 205–217 (2000).
12. O. Gascuel, BIONJ: an improved version of the NJ algorithm based on a simple model of sequence data. *Mol. Biol. Evol.* **14**, 685–695 (1997).
13. J. Waese, *et al.*, ePlant: Visualizing and Exploring Multiple Levels of Data for Hypothesis Generation in Plant Biology. *Plant Cell* **29**, 1806–1821 (2017).
14. M. Schmid, *et al.*, A gene expression map of Arabidopsis thaliana development. *Nat. Genet.* **37**, 501–506 (2005).
15. K. Nakabayashi, M. Okamoto, T. Koshiba, Y. Kamiya, E. Nambara, Genome-wide profiling of stored mRNA in Arabidopsis thaliana seed germination: epigenetic and genetic regulation of transcription in seed. *Plant J.* **41**, 697–709 (2005).
16. W. Kabsch, Automatic processing of rotation diffraction data from crystals of initially unknown symmetry and cell constants. *J. Appl. Crystallogr.* **26**, 795–800 (1993).
17. P. D. Adams, *et al.*, PHENIX: a comprehensive Python-based system for macromolecular structure solution. *Acta Crystallogr. D Biol. Crystallogr.* **66**, 213–221 (2010).
18. I. W. Davis, *et al.*, MolProbity: all-atom contacts and structure validation for proteins and nucleic acids. *Nucleic Acids Res* **35**, W375-383 (2007).